applied sciences

MDPI

Article

Investigation of the Mechanical Behaviour of Lingulid Sandstone Emphasising the Influence from Pre-Existing Structural Defects, Part 1: Model Identification Based on Static Experiments

Pascal Forquin [1], Mahdi Saadati [2,3], Dominique Saletti [1], Bratislav Lukic [1], Frederico Schiaffini [1], Kenneth Weddfelt [3] and Per-Lennart Larsson [2,*]

[1] 3SR Laboratory, University Grenoble Alpes, Domaine Universitaire, BP53, CEDEX 9, F-38041 Grenoble, France
[2] Unit of Solid Mechanics, KTH Royal Institute of Technology, 10044 Stockholm, Sweden
[3] Epiroc Rock Drills, 70225 Örebro, Sweden
* Correspondence: plla@kth.se

Abstract: A constitutive model able to describe both tensile damage and plastic deformation under confinement is a prerequisite to numerically simulate the behaviour of sandstone rock under an impact loading induced in a percussive drilling process. Therefore, model identification under both tensile and high confinement states is needed. In the present work, an experimental investigation was carried out in order to determine the mechanical properties of a sandstone rock for the purpose of advanced constitutive model identification. Different testing methods were used in quasistatic and dynamic loading regimes. This first part of the study is dedicated to static experiments, whereby three-point bend tests were first performed to evaluate the quasistatic tensile strength of the rock and its distribution by employing the Weibull statistics. Secondly, direct compression tests were conducted to evaluate the stiffness and strength in an unconfined condition. Afterwards, quasioedometric compression (QOC) tests were carried out in order to obtain the deviatoric and volumetric behaviours of the material as a function of the hydrostatic pressure (up to 375 MPa). In these QOC tests, the metallic confinement cell was instrumented with strain gauges to deduce the state of the stress and strain within the sample. A linear volumetric response along with a continuous increase of strength with the level of hydrostatic pressure was observed. This experimental work points out that, under unconfined loading (three-point bending and uniaxial compression), pre-existing structural defects play a major role leading to a highly scattered behaviour in terms of sample stiffness and ultimate applied load. On the other hand, under high confinement levels (QOC tests), beyond the nonlinear response of the curve foot, the influence from structural defects was observed to be small.

Keywords: sandstone; static experiments; constitutive behaviour

Citation: Forquin, P.; Saadati, M.; Saletti, D.; Lukic, B.; Schiaffini, F.; Weddfelt, K.; Larsson, P.-L. Investigation of the Mechanical Behaviour of Lingulid Sandstone Emphasising the Influence from Pre-Existing Structural Defects, Part 1: Model Identification Based on Static Experiments. *Appl. Sci.* **2022**, *12*, 10806. https://doi.org/10.3390/app122110806

Academic Editors: Chengzeng Yan and Gang Wang

Received: 15 September 2022
Accepted: 15 October 2022
Published: 25 October 2022

1. Introduction

The aim of this study is to investigate the behaviour of Lingulid sandstone rock, with percussive drilling as the main application of interest. Different testing methods were used in quasistatic and also dynamic loading regimes [1]. The fragmentation process generated in geomaterials under percussive loading corresponds to both (mode I and mode II) fracturing modes induced by tensile stresses and triaxial stress states. For this reason, it is necessary to consider different constitutive laws that are able to describe both tensile damage and the confined compression response. One possible candidate for such a constitutive law is the so-called KST–DFH model. The KST elastoplastic model [2,3] can be considered to model the confined behaviour of geomaterials and the tensile behaviour can be described with the DFH probabilistic-damage model [4,5] that takes into account the critical defects associated to the geomaterial. The KST–DFH model was previously used to

simulate damage and deformation modes in concrete structures when subjected to impact loading [6–8] in which high-strain-rate tensile stresses and triaxial stresses were involved. The KST–DFH model was also successfully employed in a numerical study of granite rock fragmentation of percussive drilling [9]. As explained in these previous works, the main parameters of both models can be identified based on static experiments.

As detailed in [5], the DFH multiscale model allows one to describe the probabilistic behaviour of brittle materials under low stress rates and the deterministic response at high stress rates. At low stress rates, a failure stress randomly drawn according to the Weibull model provides the ultimate strength of the considered elementary volume. At high stress rates, a damage variable is used to describe the fragmentation process involved in brittle materials at high strain rates in terms of crack inception, crack propagation, and obscuration of critical defects from propagating cracks (Figure 1a). Crack inception phenomenon can be described again according to a Weibull distribution where the density of critical defects is a power law of the applied stress $\sigma(T)$ Equation (1). In this equation, the input parameters are m, the Weibull modulus and $\lambda_0(\sigma_0)^{-m}$, the scale Weibull parameter. Both Weibull parameters can be identified from a series of bending tests (about 20 tests) [4,5]. In the DFH model, a constant crack speed V_{crack} is usually assumed for crack propagation. The last mechanism, called the obscuration of critical defects, corresponds to a shielding process from propagating cracks. It results from release waves initiated on the lips of the crack. The release of stresses in the vicinity of the propagating cracks prevents the activation of other critical defects located in a zone called the "obscuration zone" that is assumed to grow in a self-similar way. Therefore, the size of the obscured volume $V_o(T-t)$ can be expressed as function of Equation (2) (in a case of 3D volume) where V_{crack} is the crack speed ($V_{crack} = 0.38\sqrt{E/\rho}$) is assumed with the E Young's modulus and ρ the initial density), S is a shape parameter (equal to 0.38, cf. [4,5]), T is the current time, and t is the crack inception time. Finally, a damage variable is proposed (Equation (3)) taking into account the distribution of critical defects (Equation (1)) and the growth of the obscuration zones (Equation (2)). Three damage variables are defined, one for each principal direction. This makes the DFH model an anisotropic damage model.

On the other hand, the KST model provides a description of both volumetric and deviatoric behaviours of geomaterials (rocks and concrete) under confining pressure, where the deviatoric response corresponds to the increase of the maximum principal stress difference as function of the hydrostatic pressure (defined as minus the mean of principle stresses) and the volumetric response is defined as the change of volumetric strain (compaction) as a function of the hydrostatic pressure. In the deviatoric part, the locus of the yield surface is a quadratic function of the mean pressure in the principal stress space (Equation (4)), where σ_{eq} is the equivalent (von Mises) stress, P is the hydrostatic stress, and a_0, a_1, and a_2 are constant coefficients related to the considered material (Figure 1b). A piecewise linear equation of state linking the volumetric strain to the hydrostatic stress (Figure 1b) is used to describe the collapse of pores that occurs in the case of porous rocks under high confining pressure. When all pores are closed, the material exhibits a higher bulk modulus (K_{final}) which corresponds to the compacted material. As illustrated in the present paper, both responses can be determined based on a single quasistatic, quasioedometric compression (QOC) test.

At this stage, it is necessary to mention that there exist other constitutive models, for example, the Drucker–Prager law [10], which can be utilized in particular cases when the plastic behaviour of the material deviates from the associative flow. This feature is most often described by the so-called dilation angle of the material.

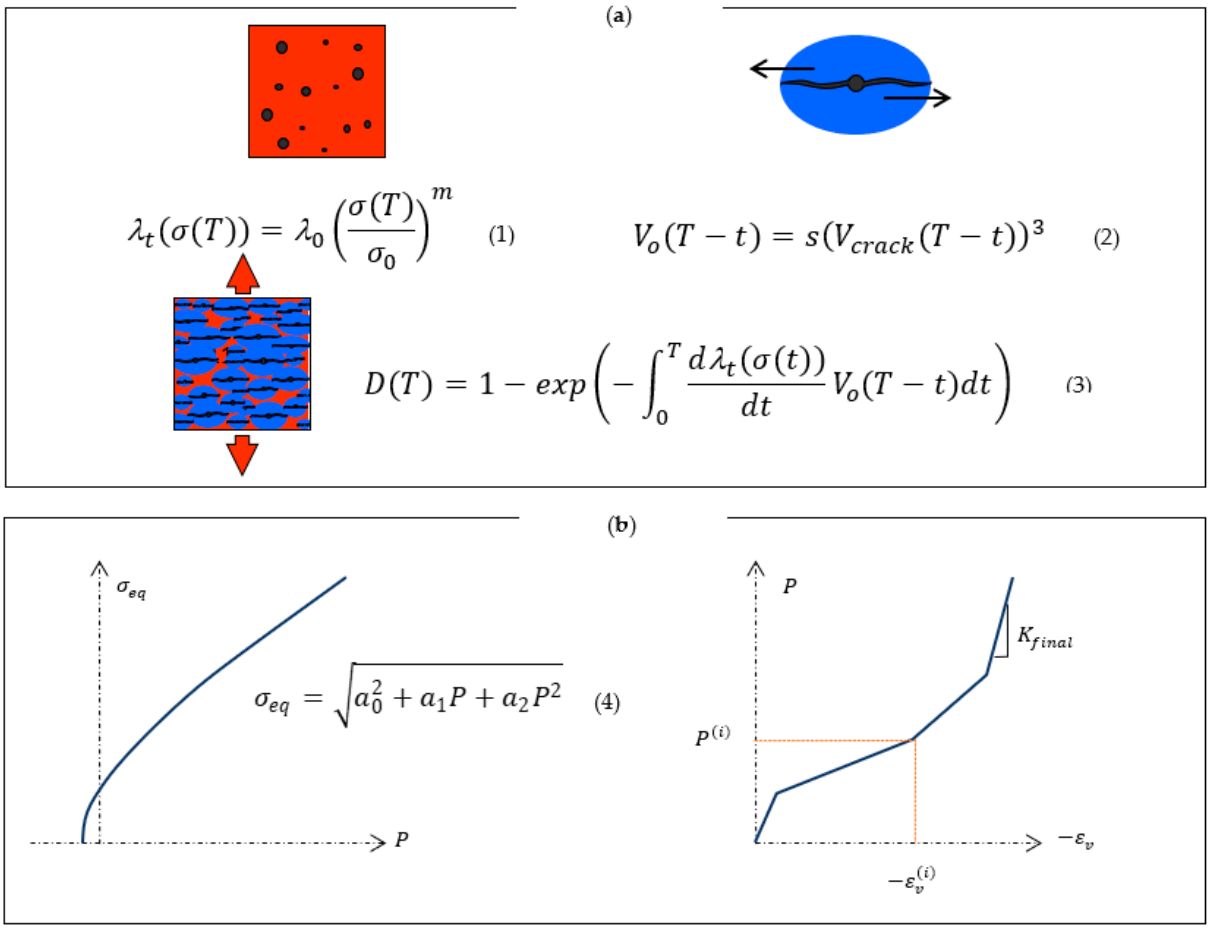

Figure 1. Description of DFH–KST coupled plasticity-damage model. (**a**) DFH (Denoual–Forquin–Hil) anisotropic damage model. (**b**) KST (Krieg–Swenson–Taylor) plasticity model.

A typical rock material that has been constitutively characterised pertinent to the KST–DFH model is granite, see [11–14]. In particular, this constitutive model was employed with the application of percussive drilling in mind. Apart from the explicit determination of material constants and functions, these investigations also showed that pre-existing (or structural) cracks have a substantial effect on the mechanical response and on the fracture pattern at, for example, impact loading. Obviously, as these investigations rely on the KST–DFH model, the material behaviour at both high- and low-strain-rate values were determined.

In a recent study, the effect on the mechanical behaviour of granite from nonassociative plastic flow was also investigated [15,16]. In particular, in [16], it was shown that the direction of the plastic flow has a significant influence on the mechanical response at spherical indentation. Indeed, not only is it important to account for nonassociativity, but also to determine change of the plastic flow direction at different values on the hydrostatic pressure. In the constitutive modelling, a Drucker–Prager law was employed together with a variable dilation angle. The influence from changing nonassociativity is, of course, a feature that can be of great interest also for other types of rock materials [17].

In the present work, an important experimental campaign was conducted using a sandstone rock provided by the international company Epiroc Rock Drills to identify the mechanical behaviour of this rock material. Three types of static experiments were used to obtain first the Weibull parameters associated to the DFH model and second the parameters related to the KST plasticity model describing the response under high confinement. In particular, a comparison between the results from the direct compression tests and quasioedometric tests highlights the influence from structural defects at different loading conditions. It should be emphasized that, although many of the experiments

conducted are designed to determine material parameters in the above-discussed KST–DFH material model, the obtained results can also be used for a complete mechanical material description when other types of constitutive models are considered. Furthermore, previous works pertinent to the mechanical characterisation of sandstone are also numerous [18–22].

2. Sample Preparation

Samples are created starting from two sandstone blocks provided by Epiroc Rock Drills: one cubic, see Figure 2, and the other cylindrical. By analysing the fracture pattern, it is possible to observe that the cubic block contains several pre-existing cracks that are spreading along the whole block. The different colours of the rock give us indicative information about the bedding planes associated to the material deposition. From the cylindrical block, cylindrical specimens are cored for the compression tests and quasi-oedometric tests. This block seems to present a different mineral composition and crack pattern when observing the surface. However, it does not present large defects and there is no evidence of bedding planes in the volume. Each sample has been rectified with a rectifier machine to guarantee the correct parallelism and planar surfaces in the samples.

Figure 2. Block of sandstone provided from the Epiroc Rock Drills.

The block chosen for the three-point bending test is the cubic one. To evaluate the characteristics associated to the rock material avoiding the pre-existing defects, each sample has been cut along the same direction starting from the same face. Each sample has been rectified by using abrasive paper to guarantee a planar surface for the supports.

In the following sections below, three types of static tests performed presently are described. To summarize, the static experimental campaign is composed of:

- Eighteen three-point bending tests;
- Four uniaxial compression tests;
- Five quasioedometric tests using a Schenk press.

3. Three-Point Bending Tests

The tensile failure of brittle materials depends on the microstructure in terms of the flaw density and failure stress distribution [23]. A series of three-point bending tests were conducted to characterise the ultimate tensile strength of the rock under static loading and to identify the parameters for the DFH model (Weibull parameters). This test was performed with an Instron press 100 kN, which has a level of accuracy of 0.5% (Figure 3). The test is conducted in a set-up with a loading pin that can tilt in two directions and with two fixed supports. The test is displacement-driven, and for this reason it is possible to investigate the crack evolution. The velocity is assigned to V = 3.6 µm/min and it is sufficiently slow to avoid any dynamic effect, and the results are captured each 0.1 s. The sample has a loaded volume $b \times h \times L = 20 \times 40 \times 120$ mm^3 and is positioned in a way to guarantee at least 20 mm out of the pins support. Several specimens presented different pre-existing cracks before the test. For this reason, the tensile surface was chosen in order to avoid their presence on the tensile surface. The tensile strength is calculated based on the nominal stress given by three-point bend test theory according to:

$$\sigma_{max} = \frac{3F_{max}L}{2bh^2} \tag{5}$$

where F_{max} is the maximum applied load. From the experimental results, it is possible to observe that the maximum load varies from 121 N to 605 N, providing tensile strengths ranging from 0.673 MPa to 2.98 MPa. The reason behind the large difference in the results is most certainly due to the presence of structural defects and pre-existing cracks. In a large part of experiments, a failure crack develops near the middle support, so in the region where the maximum tensile stress is reached. However, it is observed that when pre-existing cracks are close to the middle support, they can drive the specimen to failure (cf. Figure 4). The bending tests results are listed in Table 1. It should be clearly mentioned that when structural defects and pre-existing cracks are present, Equation (5) only gives a qualitative measure on the tensile strength.

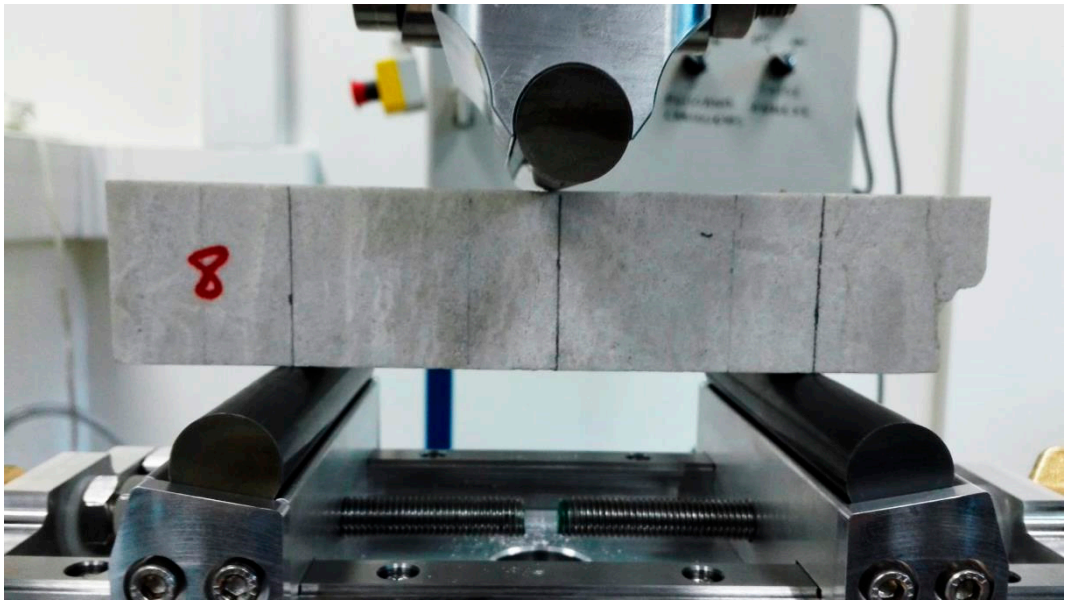

Figure 3. Set-up used for bending tests.

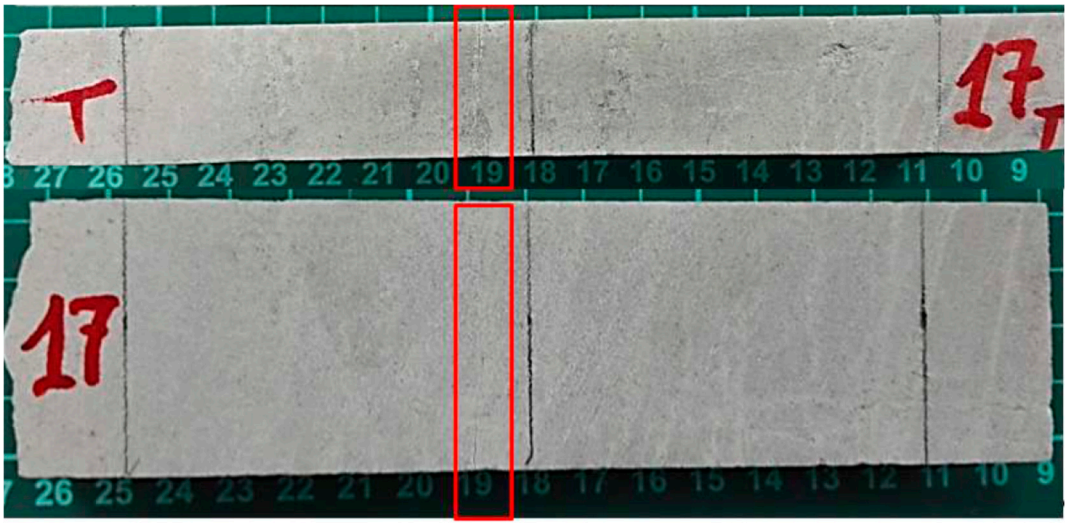

Figure 4. Crack pattern after the three-point bending in the sample #17. Top view: specimen before the test. Bottom view: tensile face and front face after the test. The structural defect that led to the failure appears in the red box.

Table 1. Results of bending tests conducted with the sandstone rock.

Sample	Rank	σ_f [MPa]	$\ln(\sigma_f)$	$P_f = (i - 0.5)/N$	$\ln(-\ln(1 - P_f))$	σ_w [MPa]
#2	1	0.673	−0.396	0.028	−3.569	2.01
#13	2	1.011	0.011	0.083	−2.442	m
#7	3	1.133	0.125	0.139	−1.900	2.77
#14	4	1.139	0.130	0.194	−1.531	V_{eff} [mm^3]
#17	5	1.334	0.288	0.250	−1.246	3377
#12	6	1.439	0.364	0.306	−1.009	
#15	7	1.660	0.507	0.361	−0.803	
#5	8	1.997	0.692	0.417	−0.618	
#3	9	2.053	0.720	0.472	−0.448	
#10	10	2.069	0.727	0.528	−0.287	
#18	11	2.194	0.786	0.583	−0.133	
#1	12	2.401	0.876	0.639	0.018	
#6	13	2.637	0.970	0.694	0.170	
#4	14	2.787	1.025	0.750	0.327	
#9	15	2.793	1.027	0.806	0.493	
#8	16	2.877	1.057	0.861	0.680	
#11	17	2.985	1.094	0.917	0.910	
#16	18	2.989	1.095	0.972	1.276	

The probability of failure P_f associated to each test is calculated by sorting the experimental results of tensile failure stress. The function $Y = \ln(-\ln(1 - P_f))$ is plotted as function of the logarithm of tensile failure stress in Figure 5, from which the slope corresponding to the Weibull modulus is deduced. The effective volume is calculated by using the formula:

$$V_{eff} = \frac{bhL}{2(m+1)^2} \quad (6)$$

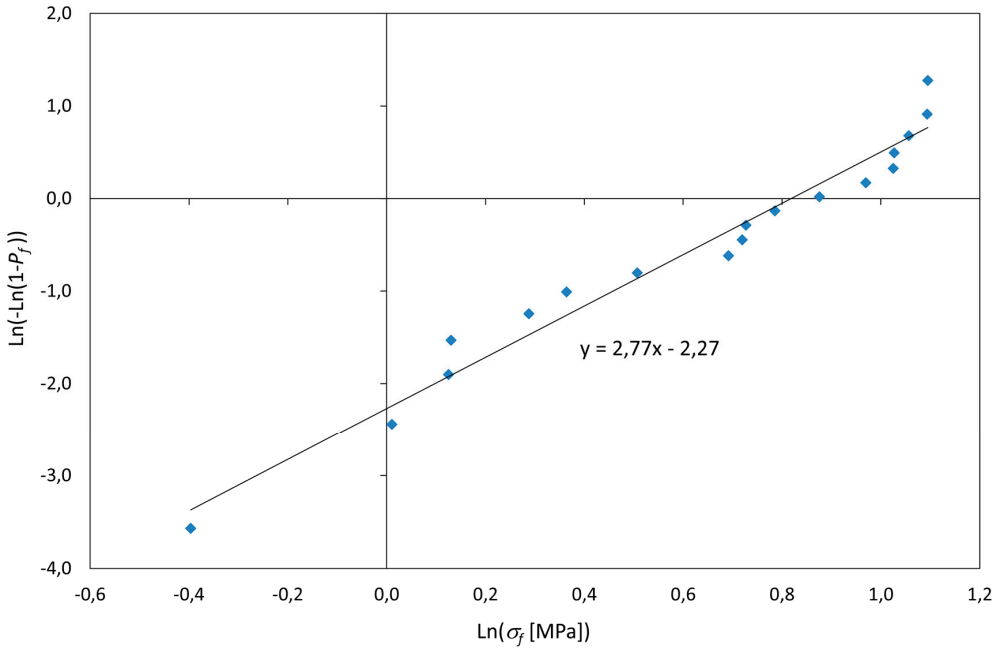

Figure 5. Graphical fitting of the Weibull distribution, where P_f denotes the failure probability and σ_f denotes each failure stress calculated according to Equation (5).

The obtained Weibull parameters are the following:
Weibull modulus: m = 2.77
Mean strength: σ_w = 2.01 MPa
Effective volume: V_{eff} = 3377 mm^3
The low Weibull modulus corresponds to the strong scatter in the obtained failure stresses.

4. Direct Compression Tests

The compressive apparatus used for the direct compression tests is a Schenck press of maximum capacity: 1 MN. The test is displacement-driven to compute the postpeak behaviour of the material. A LVDT is placed to provide an external measurement of the displacement (see Figure 6). A knee join is used to compensate any parallelism defect between contact surfaces. The velocity assigned to the press was 0.05 to 0.07 mm/s. The specimens used in direct compression tests are cylinders, 45.4 mm in diameter and 140 mm in length, cored out from large blocks by drilling and with ground ends. The selected height–diameter ratio, about 3:1 (3.08), exceeds the value usually considered (2:1) to better observe the influence of potential structural defects. However, according to several authors, the effect of length-to-diameter ratio of a rock core specimen on uniaxial compressive strength (UCS) is concluded to be small in the range (2:1–3:1) [24]. In addition, since uniaxial compression tests are not used directly in the identification of the KST–DFH model, the length-to-diameter ratio is not studied further.

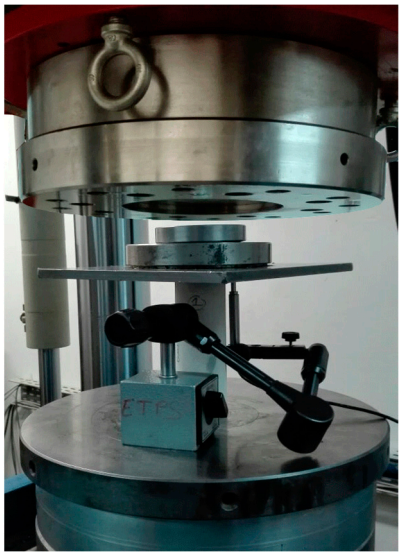

Figure 6. Compression test setup used with the Schenck press in 3SR lab.

The experimental results are gathered in Table 2. The stress–strain curves of specimens #1, #2, #3, and #5 are plotted in Figure 7. All of them exhibit a nonlinear response up to about 30 MPa. Afterwards, the response becomes linear until the peak providing a quasistatic Young's modulus in compression of about 32.06 GPa in average value. The very low compression strength of test #5 is assumed to be the result of a structural defect that initiates the macroscopic failure in compression, and accordingly may not be considered as a valid material property. In conclusion, despite the care taken to perform these experiments, uniaxial compression tests show significant variations in the measured Young's modulus and important scatter regarding the ultimate strengths and stress–strain curve foots that are supposed to result from structural defects within the tested samples. Both the nature of structural defects (thickness, length, and cohesion strength) and their orientation might have contributed to the scatter observed regarding the peak and prepeak response. The strain corresponding to the curve foot (ranging from 7×10^{-4} to 1.4×10^{-3}) could correspond to one or two horizontal structural defects with an opening of 0.1 mm. This gap will be considered as input in a numerical simulation in a parallel study [1].

Table 2. Results of simple compression tests.

Sample	Max Force (kN)	Compression Strength (MPa)	Young's Modulus (GPa)	Stress Rate (MPa/s)
#1	105.3	65.06	30.33	3.12
#2	169.5	104.98	38.87	1.50
#3	125.4	77.49	27.04	1.22
#5	58.25	35.86	32.00	1.22
Average		70.85	32.06	1.765

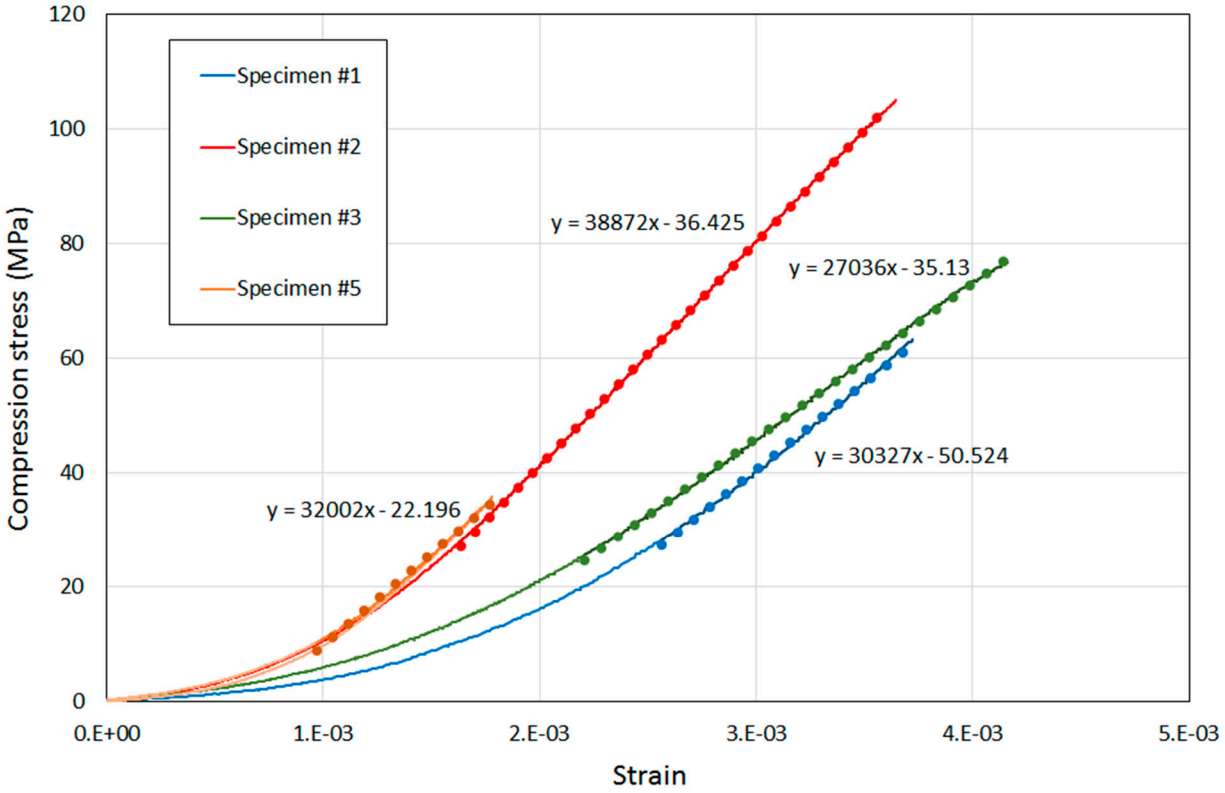

Figure 7. Uniaxial compression tests performed with 4 sandstone specimens (Table 2).

5. Quasioedometric Compression Tests

The behaviour of sandstone rock under high confining pressure was investigated in the present work by means of a quasistatic quasioedometric test [25]. The vessel is designed with an internal radius of 40.40 mm and a height of 60 mm, and it is made of very-high-yield-stress stainless steel. The setup for the test is realised in several steps: each sample is first rectified with a rectifier to ensure planar and parallel top and bottom surfaces. The cylindrical surface of the sample is covered with a thin layer of Chrysor® (which is an epoxy bicomponent resin) to eliminate any internal gap. In this way, any possible error related to geometrical defects becomes negligible. At this point, the sample is gently directed toward the vessel, and after 24 h, the setup can be tested. A special experimental device, developed in [26], is used to guarantee the centring of the vessel, fixing at the same time the two plugs (see Figure 8a).

The experiments have been performed with a Schenk press. The test is displacement-driven with a velocity v = 6 µm/s until reaching an axial force fairly close to the maximum load of the operating capacity of the machine (about 1 MN). Vertical strain in the sample $\varepsilon_{axial}^{(spec)}$ is measured from three independent LVDTs after subtracting the displacement resulting from the press stiffness deduced from the applied load. The vessel is instrumented with three strain gauges so the external hoop strain is measured ($\varepsilon_{\theta\theta}^{z=0}$, $\varepsilon_{\theta\theta}^{z=\pm 22.5}$) at three positions along the vessel axis: one strain gauge is placed in the middle of the vessel (z = 0) and two strain gauges are located near the top and bottom surfaces (z = ±22.5 mm) to control the barrelling of the confining cell (Figure 8b).

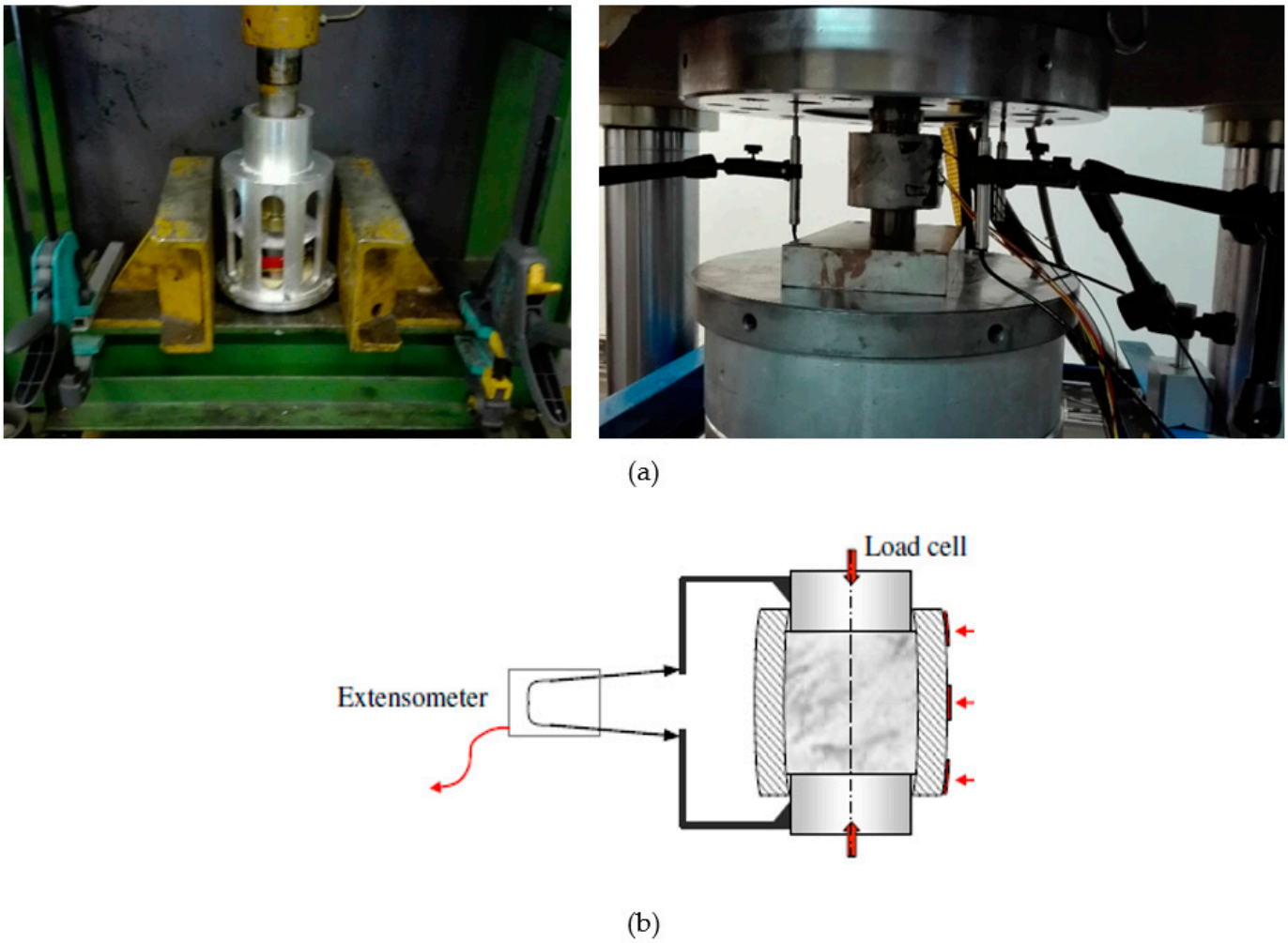

Figure 8. Quasioedometric compression testing method. (**a**) Experimental set-up. (**b**) Scheme of the instrumentation.

A series of numerical simulations were conducted to deduce the relationship between the inner radial stress at the sample–ring interface as function of the hoop strain on the outer surface of the ring ($\varepsilon_{\theta\theta}^{z=0}$) and the sample height (h) that is deduced from the initial sample height h_0 and sample axial strain. The identification procedure and related assumptions are described in [25]. The obtained equation is the following:

$$\sigma_{radial}^{(spec)} = -P_\sigma(h)\varepsilon_{\theta\theta}^{z=0} \text{ with } P_\sigma(h) = a_2h^2 + a_1h + a_0 \quad (7)$$

In the case of steel ring with an inner radius of 40.40 mm, an outer radius of 80 mm, and a height of 60 mm, the following parameters should be used: $a_2 = 1.06{\cdot}10^{14}$, $a_1 = -1.2{\cdot}10^{13}$, $a_0 = 6.19{\cdot}10^{11}$. In the same way, the average radial strain in the sample can be deduced from the outer hoop strains and as a function of the axial strain considering the barrel effect [25]:

$$\varepsilon_{radial}^{(spec)} = \frac{2}{3}\left(1 - \varepsilon_{axial}\left(1 + \frac{\varepsilon_{axial}}{2}\right)\right)\alpha_0^0\varepsilon_{\theta\theta}^{z=0} + \frac{(1+\varepsilon_{axial})^2}{3}\alpha_{25}^{22.5}\varepsilon_{\theta\theta}^{z=22.5} \quad (8)$$

where α_0^0 and $\alpha_{25}^{22.5}$ are the parameters set based on a numerical simulation describing the barrelling deformation of the ring (α_0^0 = 2.745, $\alpha_{25}^{22.5}$ = 2.20). Once the radial strain of the specimen is known, the average axial stress may be computed:

$$\sigma_{axial}^{(spec)} = -\frac{F_{axial}}{A_0(1+\varepsilon_{radial})^2} \tag{9}$$

where A_0 is the initial specimen's section area and F_{axial} is the axial force applied to the specimen, obtained either from the press load sensor. Finally, the hydrostatic pressure, the deviatoric stress, and the volumetric strain within the sandstone sample are deduced:

$$P^{(spec)} = -\frac{\sigma_{axial}^{(spec)} + 2\,\sigma_{radial}^{(spec)}}{3} \tag{10}$$

$$\sigma_{dev}^{(spec)} = \left|\sigma_{axial}^{(spec)} - \sigma_{radial}^{(spec)}\right| \tag{11}$$

$$\varepsilon_{vol}^{(spec)} = \varepsilon_{axial}^{(spec)} + 2\,\varepsilon_{radial}^{(spec)} \tag{12}$$

Finally, the deviatoric stress can be plotted as function of the hydrostatic pressure providing the deviatoric response, and the hydrostatic pressure can be plotted as function of the volumetric strain providing the volumetric response.

This testing technique and processing methodology was successfully applied to the static or dynamic characterisation of the confined behaviour of microconcrete [26,27], common and high-strength concrete [28,29] and granite rock [12] under hydrostatic pressure up to 800 MPa. Five experiments were conducted in the present work. The initial dimensions and calculated density of the samples are gathered in the Table 3.

Table 3. Initial dimensions and calculated density of the samples tested in quasioedometric compression.

Test	h (mm)	d (mm)	Mass (g)	Density (kg/m^3)
#1	49.07	40.01	149.9	2430
#2	50.05	40.30	145.5	2280
#3	49.74	40.33	153.1	2409
#4	50.09	40.38	152.1	2371
#5	49.83	40.27	150.6	2372
Average				2372.4

The change of axial stress, radial stress, deviatoric stress, and hydrostatic pressure provided in test #1 are reported in Figure 9. As in the uniaxial compression tests, despite carefully subtracting the nonlinear displacement resulting from the press stiffness, a nonlinear response is observed in the first 50 MPa of axial stress. Beyond this point, both axial and radial stresses are continuously increasing. However, given the small level of radial stress compared to axial stress, the deviatoric stress reaches 600 MPa for a hydrostatic pressure of 300 MPa. The deviatoric responses (change of deviatoric stress as function of the hydrostatic pressure) of tests #1 to 5 are compared in the Figure 10a. Above 100 MPa, the increase of deviatoric stress with hydrostatic pressure is observed to be almost linear. Finally, at a given pressure of 300 MPa, the difference of deviatoric stress (comparing samples #5 and #2) is less than 10% that is really low compared to the scatter observed in bending and uniaxial compression tests. The hydrostatic pressure is plotted as function of the volumetric strain in the Figure 10b. The nonlinear foot of the curve can be explained by a mechanism of pre-existing crack closure. Next, a linear response is observed with a slope (bulk modulus) of about 21.6 GPa. A change of slope seems to appear from 250 to 280 MPa, respectively, in specimens #1 and 2. However, higher level of hydrostatic pressure

should be considered to confirm of this change would correspond to a real mechanism (pore collapse, crack closure).

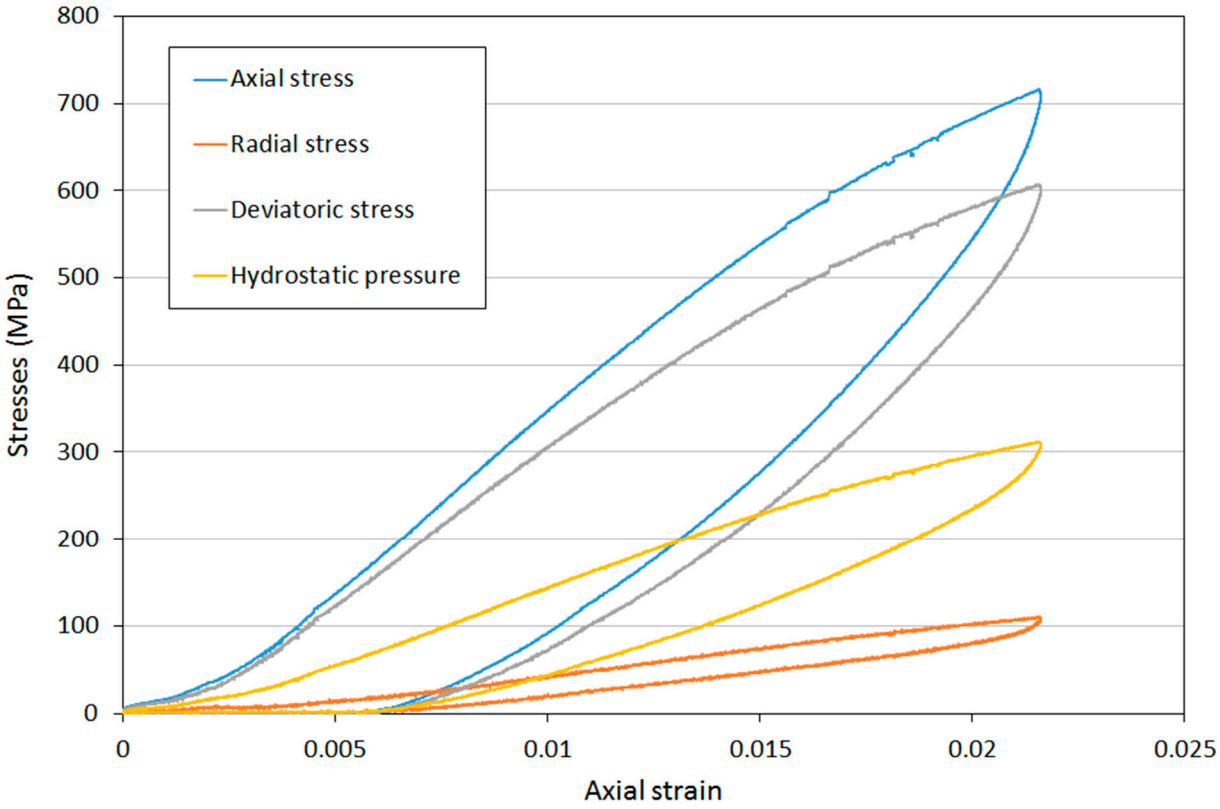

Figure 9. Stress versus axial strain in sandstone sample #1 (loading–unloading).

The maximum values of axial strain, axial stress, radial strain, radial stress, deviatoric stress, and hydrostatic stress reached during each test are gathered in Table 4. Note that the scatter of the results is significantly smaller in this situation, compared to uniaxial compression tests for instance, as the structural cracks are closed throughout these tests. Finally, the five experiments provide very similar confined responses. Quasioedometric tests can be used to identify the parameters associated to the KST model. The deviatoric response deduced from the KST model is compared to the experimental data of sample #1 in the Figure 10a. The considered parameters are reported in Table 5, where a_0, a_1, and a_2 are coefficients satisfying Equation (4).

According to parameters provided in Table 5, the yield strength corresponding to a uniaxial compression loading path ($\sigma_{dev}^{yield} = P/3$) would be 106.4 MPa, which is not far from the strength of sample #2 in uniaxial compression (105 MPa). The cut-off pressure (corresponding to $\sigma_{dev}^{yield} = 0$) is -2.07 MPa, which is not far from the mean tensile strength measured in bending tests (2.01 MPa).

A piecewise linear function is proposed to describe the volumetric response in the KST model (Figure 10b). The related parameters ($\varepsilon_v^{(i)}$, $P^{(i)}$) and final slope (K_{final}) are also gathered in Table 5.

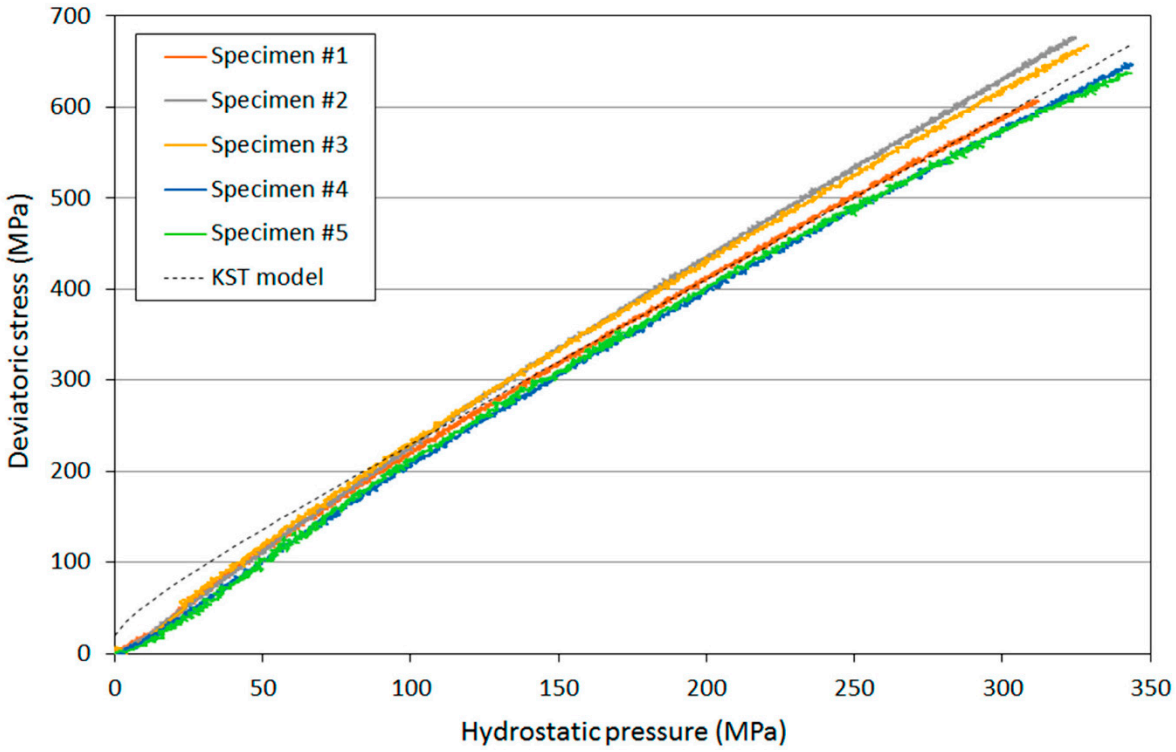

a)

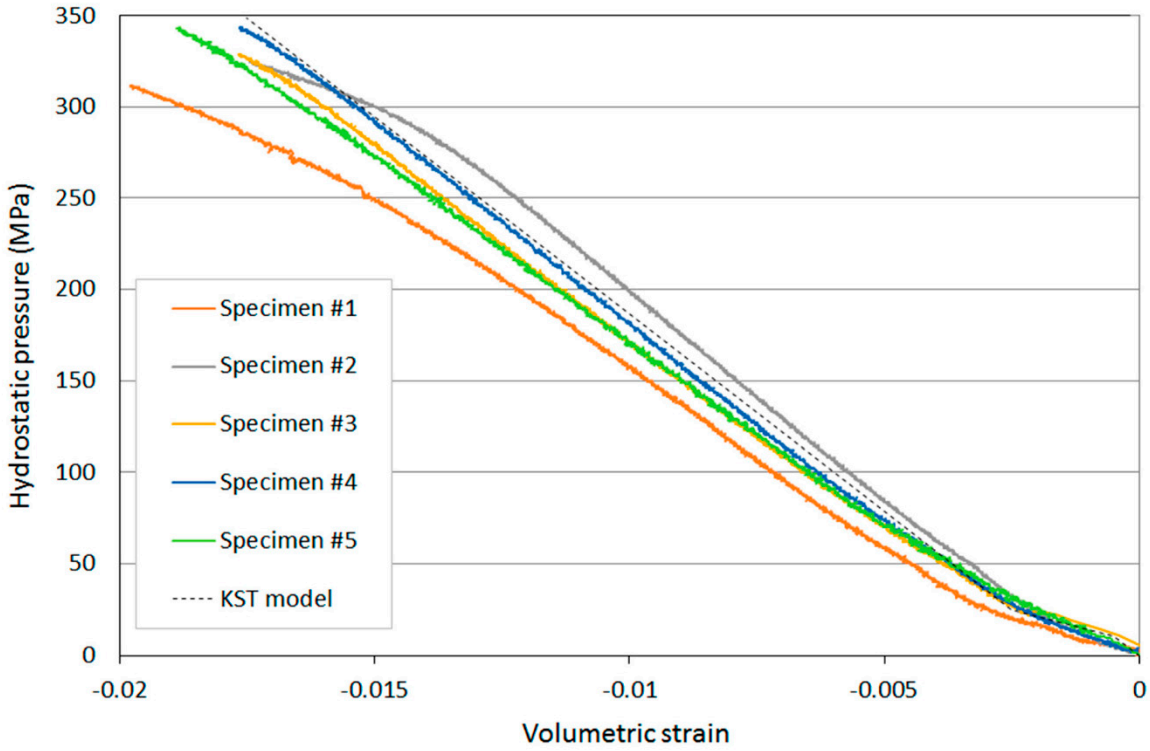

b)

Figure 10. Result of quasioedometric compression test. (**a**) Deviatoric response in sandstone samples #1 to #5 (loading); (**b**) Volumetric response in sandstone samples #1 to #5 (loading).

Table 4. Maximum values of sample radial μ-strain, axial stress, radial stress, deviatoric stress, hydrostatic pressure, and volumetric strain in quasioedometric compression tests.

Tests	Max. Axial Strain (× 1000) (abs. val.)	Max. Radial Strain (× 1000)	Max. Axial Stress (MPa) (abs. val.)	Max. Radial Stress (MPa) (abs. val.)	Max. Deviatoric Stress (MPa)	Max. Hydrostatic Pressure (MPa)	Max. Volumetric Strain (× 1000) (abs. val.)
#1	21.6	0.915	716.3	110.2	607.0	312.0	19.9
#2	18.8	0.676	775.8	101.0	677.4	325.7	17.6
#3	19.2	0.787	774.0	107.5	668.2	329.6	17.7
#4	19.5	0.882	774.9	129.0	647.6	344.0	17.8
#5	19.5	0.879	774.0	107.5	668.2	329.6	17.7

Table 5. Identification of the parameters of KST model.

Deviatoric Behaviour		Volumetric Behaviour	
$a_0(\mathrm{MPa}^2)$	400	$\varepsilon_v^{(i)}$ $(i = 1,2,3)$	$0; -5 \times 10^{-4}; -2.5 \times 10^{-3}$
$a_1(\mathrm{MPa})$	200	$P^{(i)}$ (MPa)	0; 10.8; 25
a_2	3.2	K_{final} (GPa)	21.6

6. Conclusions—Identification of the KST–DFH Model Based on Static Experiments

In a percussive drilling process, tensile stresses and highly confined stress states are induced beneath the indenter. In the present work, three types of static experiments were conducted in order to identify the parameters of the KST–DFH model in view of modelling a sandstone rock subjected to impact loading or indentation operation. The results can be summarised as follows:

On the one hand, bending tests have been conducted to characterise, respectively, the quasistatic tensile strength of the sandstone rock. These tests showed an elastic–brittle response with a strong scatter on the failure stresses, confirming the relevance of the DFH constitutive model to represent this behaviour. The experimental data demonstrates the major influence played by structural defects leading to low strength and high scatter, obviously complicating material characterisation in view of identifying a given constitutive model.

In the same way, uniaxial compression tests show a nonlinear response in the curve–foot part along with highly scattered Young's modulus and ultimate strength, again illustrating the influence of structural defects.

On the other hand, quasioedometric compression tests conducted to characterise the deviatoric and volumetric responses of sandstone at hydrostatic pressure up to 350 MPa show a continuous increase of deviatoric strength and a quasilinear volumetric response with a slope close to the expected elastic bulk modulus once the curve–foot is exceeded. In addition, the results of the five tests are remarkably reproducible. In conclusion, under confinement, the influence of structural defects seems to be small. This is in sharp contrast to the situation at uniaxial compressive testing and bending testing where the strength of the material varies considerably due to structural defects. Finally, the observed pressure-dependent response is well caught by the KST constitutive model.

In conclusion, according to static experimental results, it is concluded that in unconfined situation pre-existing structural defects play a major role in the response of Lingulid sandstone. On the other hand, under confinement, these structural defects have a much smaller influence. Therefore, these defects have to be accounted for in the model identification strategy prior to simulating numerically any industrial process such as percussive drilling. The influence of structural defects at high loading rates is discussed in a parallel paper [1].

Author Contributions: All authors have contributed to conceptualization, methodology, software, validation, formal analysis, investigation, resources, data curation, writing—original draft preparation, writing—review and editing, visualization. Supervision and project administration was led by P.F. All authors have read and agreed to the published version of the manuscript.

Funding: The research received no external funding.

Data Availability Statement: Not applicable.

Conflicts of Interest: The authors declare no conflict of interest.

References

1. Forquin, P.; Saadati, M.; Saletti, D.; Lukic, B.; Schiaffini, F.; Weddfelt, K.; Larsson, P. *Investigation of the Mechanical Behavior of Lingulid Sandstone Emphasizing the Influence from Pre-Existing Structural Defects. Part 2: Dynamic Testing and Numerical Modelling*; 2022; *Submitted*.
2. Krieg, R.D. *A Simple Constitutive Description for Soils and Crushable Foams*; Report SC-DR-7260883; Sandia National Laboratories: Albuquerque, NM, USA, 1978.
3. Swenson, D.V.; Taylor, L.M. A Finite Element Model for the Analysis of Tailored Pulse Stimulation of Boreholes. *Int. J. Numer. Anal. Methods Geomech.* **1983**, *7*, 469–484. [CrossRef]
4. Denoual, C.; Hild, F. A Damage Model for the Dynamic Fragmentation of Brittle Solids. *Comput. Methods Appl. Mech. Eng.* **2000**, *183*, 247–258. [CrossRef]
5. Forquin, P.; Hild, F. *A Probabilistic Damage Model of the Dynamic Fragmentation Process in Brittle Materials*; Elsevier Inc.: Amsterdam, The Netherlands, 2010; Volume 44, pp. 1–72.
6. Blasone, M.; Saletti, D.; Baroth, J.; Forquin, P.; Bonnet, E.; Delaplace, A. Ultra-High Performance Fibre-Reinforced Concrete under Impact of an AP Projectile: Parameter Identification and Numerical Modelling Using the DFHcoh-KST Coupled Model. *Int. J. Impact Engl.* **2021**, *152*, 103838. [CrossRef]
7. Forquin, P.; Sallier, L.; Pontiroli, C. A Numerical Study on the Influence of Free Water Content on the Ballistic Performances of Plain Concrete Targets. *Mech. Mater.* **2015**, *89*, 176–189. [CrossRef]
8. Forquin, P. Damage in Concrete Subjected to Impact Loading. In *Handbook of Damage Mechanics*; Springer: Cham, Switzerland, 2022; pp. 551–577.
9. Saadati, M.; Forquin, P.; Weddfelt, K.; Larsson, P.-L.; Hild, F. A Numerical Study of the Influence from Pre-Existing Cracks on Granite Rock Fragmentation at Percussive Drilling. *Int. J. Numer. Anal. Methods Geomech.* **2015**, *39*, 558–570. [CrossRef]
10. Drucker, D.C.; Prager, W. Soil Mechanics and Plastic Analysis or Limit Design. *Q. Appl. Math.* **1952**, *10*, 157–165. [CrossRef]
11. Saadati, M.; Forquin, P.; Weddfelt, K.; Larsson, P.L.; Hild, F. On the Mechanical Behavior of Granite Material with Particular Emphasis on the Influence from Pre-Existing Cracks and Defects. *J. Test. Eval.* **2018**, *46*, 33–45. [CrossRef]
12. Saadati, M.; Forquin, P.; Weddfelt, K.; Larsson, P.L.; Hild, F. Granite Rock Fragmentation at Percussive Drilling—Experimental and Numerical Investigation. *Int. J. Numer. Anal. Methods Geomech.* **2014**, *38*, 828–843. [CrossRef]
13. Olsson, E.; Jelagin, D.; Forquin, P. Computational framework for analysis of contact-induced damage in brittle rocks. *Int. J. Solids Struct.* **2019**, *167*, 24–35. [CrossRef]
14. Saadati, M.; Forquin, P.; Weddfelt, K.; Larsson, P.L. On the Tensile Strength of Granite at High Strain Rates Considering the Influence from Preexisting Cracks. *Adv. Mater. Sci. Eng.* **2016**, *2016*, 6279571. [CrossRef]
15. Tkalich, D.; Fourmeau, M.; Kane, A.; Li, C.C.; Cailletaud, G. Experimental and Numerical Study of Kuru Granite under Confined Compression and Indentation. *Int. J. Rock Mech. Min. Sci.* **2016**, *87*, 55–68. [CrossRef]
16. Shariati, H.; Saadati, M.; Bouterf, A.; Weddfelt, K.; Larsson, P.L.; Hild, F. On the Inelastic Mechanical Behavior of Granite: Study Based on Quasi-Oedometric and Indentation Tests. *Rock Mech. Rock Engl.* **2019**, *52*, 645–657. [CrossRef]
17. Saadati, M.; Weddfelt, K.; Larsson, P.-L. A Spherical Indentation Study on the Mechanical Response of Selected Rocks in the Range from Very Hard to Soft with Particular Interest to Drilling Application. *Rock Mech. Rock Eng.* **2020**, *53*, 5809–5821. [CrossRef]
18. Gowd, T.N.; Rummel, F. Effect of Confining Pressure on the Fracture Behaviour of a Porous Rock. In *International Journal of Rock Mechanics and Mining Sciences & Geomechanics Abstracts*; Elsevier: Amsterdam, The Netherlands, 1980; Volume 17, pp. 225–229.
19. Wong, T.F.; Baud, P. Mechanical Compaction of Porous Sandstone. *Oil Gas Sci. Technol.* **1999**, *54*, 715–727. [CrossRef]
20. Klein, E.; Baud, P.; Reuschlé, T.; Wong, T.F. Mechanical Behaviour and Failure Mode of Bentheim Sandstone under Triaxial Compression. *Phys. Chem. Earth Part A Solid Earth Geod.* **2001**, *26*, 21–25. [CrossRef]
21. Baud, P.; Vinciguerra, S.; David, C.; Cavallo, A.; Walker, E.; Reuschlé, T. Compaction and Failure in High Porosity Carbonates: Mechanical Data and Microstructural Observations. *Pure Appl. Geophys.* **2009**, *166*, 869–898. [CrossRef]
22. Wasantha, P.L.P.; Darlington, W.J.; Ranjith, P.G. Characterization of Mechanical Behaviour of Saturated Sandstone Using a Newly Developed Triaxial Apparatus. *Exp. Mech.* **2013**, *53*, 871–882. [CrossRef]
23. Amaral, P.M.; Fernandes, J.C.; Rosa, L.G. Weibull Statistical Analysis of Granite Bending Strength. *Rock Mech. Rock Eng.* **2008**, *41*, 917–928. [CrossRef]
24. Tuncay, E.; Özcan, N.T.; Kalender, A. An approach to predict the length-to-diameter ratio of a rock core specimen for uniaxial compression tests. *Bull. Engl. Geol. Environ.* **2019**, *78*, 5467–5482. [CrossRef]

25. Forquin, P.; Arias, A.; Zaera, R. An Experimental Method of Measuring the Confined Compression Strength of Geomaterials. *Int. J. Solids Struct.* **2007**, *44*, 4291–4317. [CrossRef]
26. Forquin, P.; Safa, K.; Gary, G. Influence of Free Water on the Quasi-Static and Dynamic Strength of Concrete in Confined Compression Tests. *Cem. Concr. Res.* **2010**, *40*, 321–333. [CrossRef]
27. Forquin, P.; Gary, G.; Gatuingt, F. A Testing Technique for Concrete under Confinement at High Rates of Strain. *Int. J. Impact Engl.* **2008**, *35*, 425–446. [CrossRef]
28. Piotrowska, E.; Forquin, P. Experimental Investigation of the Confined Behavior of Dry and Wet High-Strength Concrete: Quasi Static versus Dynamic Loading. *J. Dyn. Behav. Mater.* **2015**, *1*, 191–200. [CrossRef]
29. Piotrowska, E.; Forquin, P.; Malecot, Y. Experimental Study of Static and Dynamic Behavior of Concrete under High Confinement: Effect of Coarse Aggregate Strength. *Mech. Mater.* **2016**, *92*, 164–174. [CrossRef]